Stepping out of Transition Metals: Activating the Dual Atomic Catalyst through Main Group Elements

*Mingzi Sun, Hon Ho Wong, Tong Wu, Alan William Dougherty, Bolong Huang**

M. Sun, H. H. Wong, T. Wu and Prof. B. Huang
Department of Applied Biology and Chemical Technology, The Hong Kong Polytechnic University, Hung Hom, Kowloon, Hong Kong SAR, China
E-mail: bhuang@polyu.edu.hk

Dr. A. W. Dougherty
Hong Kong Applied Science and Technology Research Institute, Shatin, New Territories, Hong Kong SAR, China

Keywords: Dual atomic catalysts, Graphdiyne, Main group elements, s-p-d couplings, Machine-learning

In recent years, the investigations of atomic catalysts are in full swing. Although different atomic catalysts have been developed, the introduction of main group elements has rarely been considered. In this work, we have revealed the possibility of introducing alkaline/alkaline earth metals, post-transition metals, and metalloids to form stable graphdiyne-based dual atomic catalysts (GDY-DAC). The main group elements not only play as a promising separator to improve the loading of DAC but also activate the alkyl chain to facilitate the electroactivity of GDY-DAC. Most importantly, the main group elements to the GDY-DAC do not affect the electroactivity of transition metals or lanthanide metals and even enable subtle modulations on the electronic structures. The p band center has been a significant descriptor to modulate the electroactivity in oxide while their applications in the atomic catalysts are unclear. With the further evaluations of machine learning, it is found that the involvements of s-orbitals and p-orbitals perturb the prediction accuracies of both formation energies and p-band center, especially for the alkaline/alkaline earth metals. This work has supplied the foresight of stepping forward to the main group elements-based atomic catalysts, which opens a new avenue in designing advanced electrocatalysts.

1. Introduction

Electrocatalysts play a critical role in modern society due to the great potential for generating renewable energy and fabricating sustainable fine chemicals[1-3]. In the past few decades, numerical studies of electrocatalysts have been carried out and different advanced electrocatalysts with remarkable catalytic activity and energy utilization have been reported. Generally, transition metals (TMs) are the mainstream materials in electrocatalysts due to their versatile redox capability. The traditional design strategy of highly efficient TMs-based electrocatalysts involves the fabrication of nanosized electrocatalysts with surface electronic structure modifications through the alloying or surface strain[4-6]. Although the traditional heterogenous TMs-based electrocatalysts are promising in achieving highly efficient electrocatalysts, the applications of these electrocatalysts are limited by their high cost and poor stability. Most importantly, traditional heterogenous TMs-based electrocatalysts have an inherent limitation in metal atom utilization since only the surface atoms participate in the reaction. Although homogeneous catalysts are the better choice in maximizing the catalyst utility, they are usually suffering from poor stability and separation issues.

In recent years, massive efforts have been devoted to designing novel electrocatalysts that are able to combine the advantage of heterogenous and homogenous catalysts. Single-atom catalysts (SACs) are an ideal solution and have attracted increasing attention as highly active and efficient catalysts for electrocatalysis[7-10]. Through the atomically dispersed isolated single atoms on the supporting substrate, SACs show the maximum atom utilization efficiency, outstanding activity, explicit active site configurations[11,12]. To stabilize the isolated single atoms in the maximum loading with suppression of aggregations, Graphdiyne (GDY) has been considered to be an ideal SACs substrate due to its outstanding electrochemical properties[13-15], which is a two-dimensional carbon allotrope composing of *sp* and sp^2 hybridized carbon atoms. Such a structure allows the formation of strong covalent bondings with different single metal

atoms. The unique conjugated structure of GDY also leads to extraordinary properties including high conductivity, surface area, and stability. The anchoring of heavy metal atoms such as Pt, Pd, Rh and Ru have been intensively studied in electrochemical conversions[16-20]. Besides the transition metals, the main group elements actually have been synthesized as SAC in many previous works through the binding with support, doping and vacancies[21]. However, most of the successful SACs are mostly for thermocatalysis, in which only a few of them have been applied in electrocatalysis. Meanwhile, it has been noticed that the anchoring of main group elements has been limited to a few possible supports such as zeolite, graphene and N-doped carbon materials through the formation of Lewis pairs[22]. These previous works have fully proved the potential of main group elements to facilitate electron transfer and modify the binding strength of intermediates.

Although SACs have been proved to be highly active and efficient catalysts, their practical application is limited by the mono-atomic structure. In the practical catalytic reaction, it often occurs with more than one reactant. For instance, exhaust gas for CO oxidation contains various hydrocarbons and nitrogen oxides. In this case, the mono-atomic structure may face the significant challenge of the competitive adsorptions among reactants[23]. To overcome this challenge, multi-atomic catalysts are highly desired. Recently, dual catalysts (DAC) have been reported, where the introduction of the second metal atom enables the simultaneous adsorptions of different reactants, promotes the intermediate conversions, optimizes the binding strength, and supplies ensemble effects, improving the catalytic performances significantly[24-30]. Currently, the utilizations of TMs metals are the mainstream selections in DAC. In comparison, the main group elements including alkaline/alkaline earth metals, post-transition metals, and metalloids are rarely discussed. Owing to the high aggregation energy barrier, the post-transition metals and metalloids have great potentials in forming stable atomic catalysts[31]. Moreover, the main group elements are able to optimize the binding strengths to facilitate

electrocatalysis. For example, previous works have revealed that both the B-doped and Al-doped graphene SACs significantly improve the nitrogen reduction reaction (NRR) activity by enhancing the chemisorption of N_2[32,33]. Meanwhile, the post-TM, such as bismuth (Bi), lead (Pb), and tin (Sn), have been reported to show high electroactivity to the CO_2 reduction reactions (CO_2RR)[34-38]. Based on these works, the Bi- and Pb- SACs may also have great potential in electrocatalysis. Recently, Li's group has reported a novel SAC constructed by Bi atoms on N-doped carbon networks (Bi SAs/NC) with hierarchical porosity[34]. The Bi SAs/NC exhibit unprecedented high activity and selectivity in electrocatalytic CO_2RR when compared with the traditional Bi-based CO_2RR electrocatalyst. The latest study confirmed that the Pb-SACs can be applied in boosting the combustion of energetic fillers in solid rocket propellants[35]. Xie *et al.* also reported the atomically dispersed $Sn^{\delta+}$ sites in N-doped graphene have reached the robust and efficient CO_2RR as well [38]. Moreover, although the alkali and alkaline earth metals are not usually applied as electrocatalysts, they have been commonly used as catalysts in thermocatalysis for organic reactions, supporting their intrinsic catalytic feature [39]. Inspired by the high catalytic activity of Mg cofactors in enzymes, Liu et al. also reported that the atomically dispersed N-coordinated Mg on graphene has highly ORR electroactivity, which is comparable to the previously reported Fe-N_4 SACs [40]. They have demonstrated that the N-coordinated Mg center has the optimal binding strength with oxygenated intermediate due to the up-shift of p-band locations, indicating the main group elements are also able to activate the high electroactivity of atom catalysts.

In this work, we have applied the GDY-DAC to comprehensively investigate the thermodynamic stability and the electronic structures of the main group elements for the first time. In particular, we have focused on the significant role of p orbitals involvement in both energetic trends and the electroactivity based on the interactions among anchoring atoms and GDY (**Figure 1**). Our work has demonstrated that the main group elements show two important

roles in GDY-DAC, one is to play as a good separator to suppress aggregation of TMs and the other is to subtly modulate the *d/f* orbitals to reach the optimal binding strength for different electrocatalysis. By understanding the application of main group elements in atomic catalysts, we are able to identify a new direction of designing low-cost advanced catalysts with competitive electrochemical performances.

2. Results and Discussion

We have classified the non-transition metals and lanthanide metals into three different categories based on the periodic table including alkaline/alkaline earth metals, post-transition metals and metalloids. Alkaline/alkaline earth metals (AAEM) include 10 metal elements: Li, Na, K, Rb, Cs, Be, Mg, Ca, Sr and Ba, which usually show the s electrons as their valence electrons. Thus, we considered the AAEM as the s-block element. For the post-transition metal (Post-TM), this group includes 7 metal elements including Al, Ga, In, Tl, Sn, Pb and Bi. These electronic structures of these elements are completely dominated by the p orbitals so that we considered them as the p-block group. The last group is the metalloid, which consists of 7 elements including B, Si, Ge, As, Sb, Se and Te. For the metalloid elements, both s and p orbitals contribute to the metallic electronic structure, which we considered as the s,p block group.

The different interactions between main groups and transition metal (TM)/lanthanide in GDY-DAC lead to the different electronic structures as shown in **Figure 1**. For the AAEM, these elements are mainly dominated by the s orbitals. Due to the distinct shape and directions of the orbitals, the s-d coupling effect will be very weak, leading to slight influences on the electronic structures of anchored TM. Secondly, for the Post-TM, the p-orbitals play a key role in determining the electronic structures. In such materials, two types of orbital couplings are possible, in which one is the *p-d* couplings with the TMs while the other type of couplings is

the p-p couplings with the carbon sites of GDY. Due to the increased sensitivity and range of p-orbitals, the electronic structures become more varied in different elements. Owing to the similar p orbitals, the p-p couplings in Post-TM result in strong interactions with GDY, enabling the activations of electroactivity on the alkyl chains of GDY. Moreover, the p-d couplings are slightly improved than s-d orbitals, however, it still only shows limited overlapping at the specific directions. Correspondingly, the electroactivity of TM is affected subtly. The metalloids exhibit the s,p hybridization, which suppresses the shielding effect of s electrons, causing the evident exchange-correlation effect. Therefore, the introduction of the different main group elements causes the distinct electronic interactions between anchored elements and GDY, which determines the varied functions of anchored main group elements in DAC.

The thermodynamic stability is the fundamental property to determine whether the GDY-DAC is possible to synthesize in the experiments. To investigate whether the non-transition metals and lanthanide metals are available in achieving stable GDY-DAC, we first demonstrate the formation energies of different combinations. Based on our previous works, the main group elements are located on the porous sites that coordinated with the alkyl chain, which is the most stable anchoring site for single atoms[17,41]. Notably, for the AAEM-TM based GDY-DAC, most combinations show the energetically favorable trend, except Na, Be and Mg based GDY-DAC (**Figure 2a**). We notice that the energetic trend is highly dispersive and lacks regulations between elements, which is ascribed to the strong perturbations of the local electrical field by the s-orbitals from AAEM to TM. Similarly, we notice that the energy fluctuations become even stronger in the combinations of AAEM-4d and AAEM-5d based GDY-DAC (**Figure 2b-2c**). Meanwhile, we notice the gradual increase trend of the overall formation energies. For the and AAEM-5d based GDY-DAC, not only the formation energies have increased, but also the range of formation energy becomes much larger, covering from -3 eV to 5 eV. Notably, only Au and Hg based GDY-DAC are able to form spontaneously. From 3d to 5d TM, it is found

that both Be and Mg display relatively higher formation energies, indicating the lower thermodynamic stability during the experimental synthesis. For the combinations of Post-TM with TM, the formation energies have further increased to higher than AAEM-based GDY-DAC (**Figure 2d-2f**). Due to the wider range of p orbitals in Post-TM, the perturbations to the local electronic distributions are alleviated, leading to a slightly more converged formation energy. However, the wider ranged p orbitals still impose an influence on the electrical field near d-orbitals, leading to a not completely converged energetic trend. Interestingly, for metalloid based GDY-DAC with s-p hybridized orbitals, the energetic trends are highly converged, where energy changes are limited in a small range (**Figure 2g-2i**). This indicates that the metalloid atoms are able to occupy the vacancy sites and form the "*mirror*" atom pairing with the TM without affecting the overall thermodynamic stability. These results prove the potential of metalloid as the stable separator via the "*mirror*" effect. As the atomic radius of TM increases, the formation energies increases while the converge feature is still preserved. Therefore, the metalloid atoms serve as the separator to stabilize the mono-dispersed TM and protect the GDY-DAC from aggregation or catalyst poisoning due to the overbinding effect.

In our previous works, we have identified that the introduction of lanthanide (Ln) metals lowered down the formation energies due to efficient electron transfer between d-f orbitals. To gain insights into interactions between Ln metals with AAEM, Post-TM, and metalloid, we have mapped out their formation energy trend (**Figure 3a**). Notably, the formation of GDY-DAC is mostly exothermic. In particular, we notice that the AAEM-Ln GDY-DAC has shown the lowest formation energies, in which the alkaline metal-alkaline metal based GDY-DAC demonstrates the strongest formation trend. This is due to the strong shielding effect of s-orbitals enables the over-coupling with f orbitals, which lowers the formation energies. We notice that such a phenomenon has been weakened between the Post-TM and Ln metals, in which the light lanthanide metals such as Pr still show evidently lower energy than other Ln

metals (**Figure 3b**). This is due to the weaker shielding effect in p orbitals, which leads to stronger interactions. For most of the metals, the formation energies are limited in the range of -1 eV to 1 eV (**Figure 3c**). For the metalloid group, the couplings between metalloid and Ln metals are also relatively weak and most of the formation energies are near the neutral line (0 eV). In addition, the lowest formation energies still appear at the metalloid-Pr GDY-DAC while the metalloid-Tb GDY-DAC exhibit higher energy costs. Among all the Ln metals, the light Ln metals such as Pr, Nd exhibit a lower energy cost due to the balance between s/p-f couplings and repulsive forces. Compared with TM, the majority of Ln-based GDY-DAC are energetically favorable due to the less repulsive forces between anchoring atoms. This demonstrates that the combinations between main group elements and Ln metals are able to achieve both highly stable and efficient electrocatalysts. For the 12 different combinations AAEM-3d, AAEM-4d, AAEM-5d, AAEM-Ln, Post-TM-3d, Post-TM-4d, Post-TM-5d, Post-TM-Ln, metalloid-3d, metalloid-4d, metalloid-5d, metalloid-Ln, the most stable structures have been demonstrated in **Figure S1**. It is noted that the most stable structures in AAEM-TM DAC are Ba-based DAC. Meanwhile, the interactions between metalloids and transition metals become weaker, where the two atoms evenly occupy the pore structures. Interestingly, we notice that lanthanide metals show very strong repulsive forces with both AAEM and Post-TMs, which lead to the far separations of the two atoms in different pore positions. In comparison, the interactions between the metalloid and lanthanide are alleviated and the two neighboring atoms can be stabilized within one pore. Then, we have further compared the formation energies of all the combinations. Among the 12 different combinations, the combinations with lanthanide metals have shown much lower formation energies, supporting the stable structure for experimental synthesis (**Figure S2a**). Comparing with the transition or lanthanide metal SAC, the energy differences with the DAC are shown in **Figure S2b**. For AAEM, all the DAC are much more stable than the SAC, confirming the possibility of using AAEM as the "*inert separator"* to avoid aggregation. For Post-TM, the energy differences become much smaller

and some of the DAC may be more unstable than the SAC. Moreover, the metalloids are also able to stabilize the transition metals within the DAC. Based on these results, the AAEM and metalloids are both suitable to be the inert separator in the DAC to increase the potential loading of transition metals and lanthanide.

From the overall mapping, we notice that the highest energy cost appears in the TM-TM GDY-DAC, which explains the current synthesis challenge for achieving stable DAC (**Figure 3d**). Meanwhile, even the combinations of Post-TM-TM and metalloid-TM display high energy costs. On the contrary, we notice that the Ln-based GDY DAC exhibit the most stable structures, especially with the AAEM. For combinations among AAEM, Post-TM, and metalloid elements, we notice AAEM-AAEM GDY-DAC show the highest thermodynamic stability while the formation of Post-TM-metalloid GDY-DAC is endothermic. These results further confirm that the higher thermodynamic instabilities are correlated with the sensitive p and d orbitals. The strong shielding effect of both s and f orbitals is able to alleviate the repulsive forces induced between the anchoring atoms, leading to the highly stable electrocatalysts. The formation energies of DAC formed between main group elements have been displayed in **Figure S3**. It is noted that the energy costs of AAEM-AAEM DAC are the lowest while the combinations between Post-TMs and metalloids are not energetically favored due to the high energy cost. The DAC based on combinations between alkaline metals and Post-TM or metalloids still mostly display thermodynamic stability. In comparison, the DAC based on alkaline earth metals with Post-TMs or metalloids are much less stable. These results confirm that AAEM-based DAC are the most promising candidates for experimental synthesis.

During the synthesis, there are several possible synthesis competitions in the solutions, such as the formation of homo GDY-DAC or GDY-SAC. To obtain a more in-depth understanding of GDY-DAC synthesis, we first compare the formation energy cost with homo-TM GDY-DAC

(**Figure 4a**). We notice that the homo-TM GDY-DAC are highly unpreferred during the synthesis since the energy cost of hetero-TM GDY-DAC with AAEM, Post-TM and metalloids are much lower. Among all the combinations, it is noted that the formation of Nb-Nb and Hf-Hf GDY-DAC is feasible during the synthesis due to a higher preference than hetero-Nb/Hf-based GDY-DAC. We have further summarized the energy difference in **Figure 4b**. From the AAEM to metalloid, the energy differences have been gradually become more dispersive, indicating the stronger competition between the formation of homo-TM and hetero-TM based GDY-DAC. After the Fourier transfer treatment, we notice that the peaks are gradually weakening from alkaline/alkaline earth to metalloid based GDY-DAC (**Figure 4c**). In the AAEM-based GDY-DAC, there are repeated peaks while these peaks become weaker in Post-TM and metalloid based GDY-DAC. These indicate the different behaviors between s-block materials (AAEM) and p-orbital dominated materials (Post-TM and metalloids). During the synthesis, the competitions with homo-AAEM, Post-TM and metalloids based GDY-DAC are also significant (**Figure 4d**). After comparison, it is found that metalloid based GDY-DAC display a stronger preference to form the hetero-metalloid DAC than the homo-metalloid GDY DAC. In comparison, the AAEM prefers to occupy the surface vacant sites, which are the potential to be a good separator. Then, a comparison with GDY-SAC is also needed (**Figure 4e**). Interestingly, the competition between SAC and DAC is not evident, where most of the formation energy differences are in the range of ± 1.0 eV, especially for the 3d and 4d TM. However, we notice that Se-based GDY-DAC has shown a stronger preference than the GDY-SAC, indicating the feasibility of experimental synthesis.

Besides the formation energies, the electronic structures are also highly significant to understand the influence of the introduction of alkaline/alkaline earth metals, post-transition metals and metalloids to the GDY-DAC. In particular, the p-band center has been proved that plays an important role in modulating electroactivity. However, current research mostly focuses

on the p-d orbital couplings in transition metal oxide materials. The p-p coupling has rarely been discussed. The p-band centers of AAEM in GDY-DAC constructed by s-block and p-block elements are displayed (**Figure 5a**). It is noted that the p-band centers of AAEM have only shown a very limited change even after the combination with other elements. These results are attributed to the very weak s-block couplings effect by the strong shielding effect. These demonstrate that alkaline/alkaline earth metals are relatively inert in the GDY-DAC, which are playing as the stable separator to form the coverage on the vacant sites. However, although the p-band is inert, the s-electrons in AAEM show an influence on the p-band of alkyl chains in GDY (**Figure 5b**). Notably, the alkaline ions have pushed the p-band of the alkyl chains closer to the Fermi level, which activates the electroactivity of the alkyl chains to facilitate the electron transfer. It is noted that the p-band center of Post-TM is affected by the combinations with other elements. We have noticed the fluctuations become evident in the p-band center, especially the Al, In, Sb (**Figure 5c**). The combination with Se largely lowers the p-band center of Post-TM, indicating the suppression on the p-band center. Since the p-p couplings usually are mid-range to long-range, their sensitivity to the second element becomes higher, which further results in stronger modulations on p orbitals and the electron cloud of Post-TM. In the meantime, due to the strong interactions between anchoring atoms, the modulations on the alkyl chains are weaker, leading to barely unchanged p-band (**Figure 5d**). Only the AAEM-Post-TM GDY-DAC show the upshifted p-band center of alkyl chains due to the strong effect from the s orbitals of AAEM. For the metalloid-based GDY-DAC, the p-band centers show even stronger fluctuations, which vary from below Fermi level to crossing Fermi level (**Figure 5e**). The s-p hybridizations in the metalloid alleviate the shielding effect of s electrons, which induces an even longer range of orbital couplings between the anchoring atoms, causing the evident exchange-correlation effect. This also proves the high sensitivity of p orbitals in metalloids. Due to matching between p-orbitals, the p-band centers of alkyl chains is also important, which are demonstrated in **Figure 5f**. Although the shield effects are weakened on s-orbitals, the p

orbitals still dominate the interactions with the alkyl chain. The p-band centers of the alkyl chains are not significantly affected except those that include the alkaline metals. Moreover, we notice that Se atoms activate the alkyl chain to form the highly electroactive regions, which improves the electron transfer to achieve efficient electrocatalysis.

After considering the combinations within alkaline/alkaline earth metals, post-transition metals, and metalloids, the influences on the electronic structures of transition metals and lanthanide metals are also investigated (**Figure 6a**). For the AAEM based GDY-DAC, the d-band centers still demonstrate the periodically downshifting trend in the transition metals, which are only slightly affected by the introduction of AAEM. The influences on 3d TM are not evident. However, for 4d and 5d TM, we notice that the shifting of the d-band center induced by the anchoring AAEM. The alkaline earth metals slightly downshift the d-band center than the alkaline metals, which does not change the overall d-band trend. The small adjustments to the d-band center indicate the potential to precisely modulate the electroactivity of the transition metals to avoid the over-binding effect. For the Post-TM based GDY-DAC, the d-band and f-band center become nearly converged (**Figure 6b**). The d/f band centers are not significantly affected by the introduction of Post-TM, supporting limited modulations on the electroactivity of transition metals and lanthanide metals. However, we still notice some exceptions. For example, the Al and Pb activate the Pt-5d and Au-5d significantly, improving the electron transfer by reducing the energy barrier. These results prove that p-d and p-f couplings between anchoring atoms are highly preferred, which suggest that Post-TM are appropriate separator for controlling the active site distributions in the TM/Ln based SAC without sacrificing the electroactivity of active sites. In addition, we have noticed a highly converged d/f band center in the metalloid-based GDY-DAC (**Figure 6c**). However, the introduction of Se is able to boost the electroactivity of active metal sites by uplifting their d-band center, especially in the 5d TM and Ln metals. In particular, the f-band centers for light to medium Ln metals (La ~ Tb) have

been evidently upshifted. The largest changes of f-band centers happen to Gd, Tb, and Pr in GDY-DAC. Therefore, the introductions of alkaline/alkaline earth metals, post-transition metals and metalloids do not impose a significant effect on the electroactivity of anchoring TM and Ln metals. Meanwhile, some precise minor modulations on the electroactivity of TM or Ln metals are able to accomplish by selecting the appropriate second anchoring metals.

In previous works, Shao-Horn et al. have proposed the p-band center theory to evaluate the modulations on the d-band center as well as the electroactivity [42,43]. In their works, the closer distance between band centers allows stronger modulations by more efficient electron transfer. By applying a similar concept, we also explore the orbital interactions regarding the band center differences (**Figure 7a**). The p-p band center differences represent the energetic interval from the p-band centers of AAEM, Post-TM and metalloids to the p-band center of the alkyl chains of GDY, which evaluates the interactions between introduced AAEM, Post-TM and metalloids and GDY structures. The p-d/p-f differences represent the distance from the d/f band center of TM and Ln metals to the p-band center of AAEM, Post-TM and metalloids, which reveals the interactions between two anchoring atoms. In the AAEM based GDY-DAC, although the alkyl chains are slightly modulated, the overall differences of the p-p band center are distinguished by the p-orbitals of AAEM, which shows an increasing trend from 2p to 5p orbitals. Meanwhile, the p-d/p-f band center differences show similar regulations (**Figure 7b**). Due to the large variation of p-band centers in AAEM, the band center differences also display changes in a wide range. The alkaline and alkaline earth metals show the opposite modulations to the d/f band center, which are consistent with the change of d/f-band center variations. For the p-block dominated Post-TM, the p-band centers are all located above the p-band center of the alkyl chains (**Figure 7c**). Only a few combinations between Bi and AAEM show relatively close distances, which indicates the potential modulations on the alkyl chain. Although the p-band centers of post-transition metals show fluctuations, the d-band center still dominates the

electronic structures (**Figure 7d**). The p-d/p-f differences mainly follow the variation trend of the d-band center of transition metals and lanthanide metals. Owing to the s-p hybridization, the p-band centers of the metalloid become more unstable (**Figure 7e**). This also leads to the fluctuated p-p band center difference, which may affect the potential electroactivity towards oxygen reduction or evolution reactions. For all the metalloid elements, they show higher positions of p-band center than that of alkyl chains, in which Se-based GDY-DAC display the smallest differences. These results support the activations of alkyl chains in GDY by anchoring Se atoms. Compared to the Post-TM based GDY-DAC, it is noted that the p-d/p-f band center differences have significantly increased in metalloid-based GDY-DAC (**Figure 7f**). Meanwhile, more combinations are able to modulate the electronic structures of the anchoring TM and Ln metals. However, we notice that the difference between orbitals still follows a similar trend as the d-band centers, further confirming the dominant contributions of d-orbitals in electroactivity.

Depending on our previous work, we continued to develop the use of Gaussian Process regression (GPR) due to its relatively low computation cost on smaller data sets [44] and previous success at giving promising results on our target dataset [30]. Our previous work has confirmed that machine learning is an effective tool to predict the thermodynamic stability and electronic structures of GDY-based electronic structures. To evaluate the influences of introducing p orbitals, we have also introduced the GPR algorithm method to predict both the energetic trend and electronic structures of GDY-DAC in this work. Compared to common big data, our work has a relatively small dataset, which is suitable for applying the GPR method, which also supplies the uncertainty measurements on the predictions. Among different models of GPR, we have selected the Squared Exponential GPR, which is able to handle smooth functions and discontinuities with small errors. The general expression of Squared Exponential GPR is shown below.

$$k(x_i, x_j|\theta) = \sigma_f{}^2 \exp[-\frac{1}{2}\frac{(x_i-x_j)^T(x_i-x_j)}{\sigma_l{}^2}] \quad (1)$$

In the above Eq. (1), $r = \sqrt{(x_i - x_j)^T(x_i - x_j)}$ represents the Euclidean distance between x_i and x_j, σ_f is the signal standard deviations and σ_l indicates the characteristic length scale. θ represents the covariance function. Detailed explanations are supplied in the Methods Section. In this work, we have applied the square exponential GPR for both formation energies and p-band centers of the GDY-DAC. For the formation energies and electronic structure predictions, the input dataset for training includes the mass numbers, weight, electronegativity, electronic configurations, p/d/f band centers, ionization energies, electron affinity, atomic radius, and conductivity of both anchoring atoms. The dataset includes 1356 groups of data.

The machine learning results have been displayed in **Figure 8**. For the AAEM-based GDY-DAC, the formation energies have shown prediction results with root-mean-square error (RMSE) of 1.268 (**Figure 8a-c**). From the s-block materials to the *s,p* hybridized block, the RMSE has gradually reduced from 1.268 to 0.802, indicating an increase in the accuracy of the prediction results from machine learning. These results demonstrate that the introduction of p orbitals has increased the difficulties of machine learning predictions. Compared to our previous works in TM/Ln metal based GDY-DAC, the thermodynamic stability becomes more sensitive. Accordingly, with the introduction of p orbitals, only the fundamental parameters are not able to fully reproduce the formation energies. Due to the large variation of formation energies, we notice that some edge data of formation energies show the deviated predictions (**Figure 8d-f**). Notably, the prediction accuracies in the electronic structures show a different order as Post-transition metals (p-block) > Metalloid (s,p hybridized) > Alkaline/Alkaline earth metals (s-block) (**Figure 8g-i**). The prediction accuracy varied significantly in a different group of elements. In particular, the p-band center predictions of AAEM show relatively large deviations with RMSE of 2.185, which is attributed to the large variation range of p-band

centers in AAEM with high discontinuity. The ultra-high accuracy of Post-TM may arise from the highest matching level between anchoring sites and alkyl chain, especially the p-p orbital couplings. The prediction accuracies have confirmed the higher difficulties of s-block elements due to the large variation range in both energy and band center. Correspondingly, the prediction results of the metalloid-based GDY-DAC with s,p hybridized orbitals, the RMSE has increased to 0.360, which is still much lower than that of the AAEM-based GDY-DAC. The comparison of the data shows that the main deviations of data are originated from the discontinuity region in the p-band center of AAEM-based GDY-DAC (**Figure 8j-l**). In comparison, the predicted values are highly overlapping with the DFT data in Post-TM GDY-DAC. The deviation of data in metalloid-based GDY-DAC is also noted at the edge region. Therefore, these results demonstrate that the involvements of p orbitals in DACs are not completely dependent on the intrinsic properties of anchoring atoms, where the orbital couplings between anchoring atoms and with the GDY both have induced evident effect on the p-band centers. This will supply significant references for the modulations of the electroactivity of atomic catalysts in the future.

3. Current Progress and Challenges

Currently, alkaline and alkaline earth elements have been reported as single atomic thermocatalysts in many works, where they exhibit highly acid-tailorable Lewis-base properties that can catalyze several industrially relevant reactions[45]. The most common hosts for alkaline and alkaline metals are zeolites, which apply the cation-exchange methods to achieve the atomic catalysts[22]. Through the change of the alkali metal cation sizes and the modulations of acid-base properties induced by the interactions with the host, the performances of the SAC can be promoted or reduced[46]. Among the alkaline earth metals, the stabilization of Mg single atom allows the new type of Brønsted acid sites or as a tandem base in Brønsted catalyzed reactions[47]. For the post-transition metals, the main host to achieve the atomic catalysts are also zeolite via the isolations in the “extraframework” positions and the substitution of Si atoms.

The different types of zeolites, valence states, and charge-balancing cations all lead to distinct Brønsted or Lewis acidic or oxidative functionality. It is found that the effect of Lewis acidity is strongly correlated with the valence states of post-transition metals [48]. For example, the flexible coordination environments of Al in zeolite impact both the properties and environment of the associated active site[49,50]. The metalloid based atomic catalysts show broader possible hosts covering from zeolite to carbon materials, which enables the applications from the classic Brønsted-acid catalyzed transformations to oxidations as well as the electrocatalytic reductions. In particular, the doping of boron into the carbon materials can either achieve the frustrated Lewis acid-base pairs or the directed electron transfer for different electrochemical reactions including ORR, NRR and HER[51,52]. Interestingly, the exact active site structures and catalytic roles of selenium in SACs are not fully understood, the introduction of Se enables the charge accumulation and spin polarizations, which optimizes the binding strength and improves the potential-determining step[53,54]. It is noted that most main groups are reported as the thermocatalysts for organic reactions, where their applications in electrocatalysts are still limited. Compared to the transition metals, more explorations on the synthesis methods are strongly needed for future developments of main group elements based DAC. Only a few elements such as B, Se, and Ge have been reported their applications in electrocatalysis. In this work, we have supplied a new idea that how to extend the potential of main group elements in electrocatalysts, especially the atomic catalysts. Meanwhile, based on our systematic research, we have identified that combining main group elements with TM and Ln metals is a promising strategy to synthesize the stable DAC, which not only preserves the high electroactivity due to the long-range p-orbital coupling effect but also alleviates the possible aggregation effect as the separator. Therefore, this work has supplied a novel direction to extend the applications of main group elements in the electrocatalysts, which will be very inspiring for future research works in this field.

4. Conclusion

Relying on the current developments of atomic catalysts, how to step out of the transition metals to extend the possibility of catalyst materials is a key challenge. Although few reports have reported the atomic catalysts based on the main group elements, more comprehensive research is still needed. In this work, we have investigated the main group elements-based GDY-DAC regarding both the thermodynamic stability and electronic structures. In particular, we notice that combining main group elements with TM and Ln metals are able to form the stable DAC and preserve the high electroactivity due to the long-range p-orbital coupling effect. Moreover, the machine learning technique based on the exponential GPR algorithm has further confirmed the different roles of *s* and *p* orbitals induced by the main group elements. To move forward to the synthesis of innovative atomic catalysts in future research, our work has supplied the essential theoretical reference to fresh understandings of feasible elements in atomic catalyst materials.

5. Methods

Calculation Setup: To understand the thermodynamic stability and electronic structures of GDY-DAC with main group elements, we have applied the density functional theory (DFT) through the CASTEP package [55]. For the calculations, we have selected the generalized gradient approximation (GGA) with the Perdew-Burke-Ernzerhof (PBE) functionals to describe the exchange-correlation energy [56-58]. We have set the cut-off energy to 380 eV with the plane-wave basis set and the ultrasoft pseudopotential scheme has been applied for all the geometry optimizations [59]. For the energy minimizations, the Broyden-Fletcher-Goldfarb-Shannon (BFGS) algorithm is applied for the k-point mesh [60,61]. Meanwhile, the convergence criteria for the geometry optimizations have been set as follows: the Hellmann-Feynman forces should be less than 0.001 eV/Å; the total energy should not exceed 5×10^{-5} eV per atom and the maximum atomic displacement should not exceed 0.005 Å. In this work, we have considered all the dual metal combinations between main group elements (AAEM, Post-TM, and

metalloids) with transition metals and lanthanide metals. This work has considered total 1356 combinations. For each GDY-DAC model, the 2×2×1 supercell of single-layered GDY has been applied as the substrate. Meanwhile, there are three possible anchoring sites in each unit of GDY based on our previous works [16-18,30]. The two different elements have been placed between the C2 and C3 sites of the alkyl chain in GDY, which have been proved to be the most stable position. To guarantee full relaxations, we introduce 15 Å vacuum space in the z-direction.

Machine Learning Algorithm: We can define the GPR as a probabilistic regression model based on Gaussian processes, specifically the GPR uses kernel-based nonparametric hyperparameters. Importantly we must assume that any data used for the training of the GPR are assumed to be from an unknown distribution. To further explain we can use the standard linear regression to explain the GPR conceptually. In linear regression when we have a training set of $\{(x_i, y_i); i = 1,2, \dots, n\}$, where $x_i \in \mathbb{R}^d$ and $y_i \in \mathbb{R}$ are from unknown distributions, a regression model will have the following form.

$$y = x^T\beta + \varepsilon. \tag{2}$$

Where, $\varepsilon \sim N(0, \sigma^2)$ is a zero-mean normal distribution and the error variance σ^2 and coefficients β are learned from the data using a training algorithm. A GPR differentiates itself from the linear regression equation because it representing the data using basis functions ($h(x)$) and inserting latent variables ($f(x_i), i = 1,2, \dots, n$) from a Gaussian Process (GP). To explain this, we rewrite the previous linear regression equation as below.

$$y = h(x)^T\beta + f(x) \tag{3}$$

As an important element of the GPR, the GP should be understood, as such, it can be defined by $f(x) \cong GP(0, k(x, x')$, here, $f(x)$ is approximately from a zero-mean GP with a covariance function of $k(x, x')$. Furthermore, the basis functions defined by h(x) transform the input

features into a higher dimensional feature space such that if $x_i \in \mathbb{R}^d$ is d dimensional vector then $h(x) \in \mathbb{R}^p$ and β are vectors of p length where β represents the coefficients of the basis function. When implementing the GPR we must tune the covariance function, this parameterization is labeled as θ and the covariance function is often represented as $k(x, x'|\theta)$. In this study, the GPR model was built using the Squared Exponential (SE) Kernel and then assessed using Root mean square error (RMSE) to determine the fit of the model to the training data. The SE equation can be defined as below.

$$k_{SE}(x, \acute{x}) = \sigma^2 \exp\left(-\frac{(x-\acute{x})^2}{2\ell^2}\right) \quad (4)$$

In this equation, where the hyperparameters σ and ℓ control the scale and length scale of the kernel respectively. The model was then validated using k-fold cross-validation to allow the model to be more robust, protecting from the overfitting and giving it a better idea of how well it would perform on future data. For the validation, we used a k-value of 5 as recommended for the k-folds cross-validations [62].

Supporting Information
Supporting Information is available from the Wiley Online Library or from the author.

Acknowledgements
The authors gratefully acknowledge the support of the Natural Science Foundation of China (Grant No.: NSFC 21771156), and the Early Career Scheme (ECS) fund (Grant No.: PolyU 253026/16P) from the Research Grant Council (RGC) in Hong Kong.

Received: ((will be filled in by the editorial staff))
Revised: ((will be filled in by the editorial staff))
Published online: ((will be filled in by the editorial staff))

References

[1] Seh, Z. W.; Kibsgaard, J.; Dickens, C. F.; Chorkendorff, I.; Norskov, J. K.; Jaramillo, T. F. *Science* **2017,** *355*.
[2] Ross, M. B.; De Luna, P.; Li, Y. F.; Dinh, C. T.; Kim, D.; Yang, P.; Sargent, E. H. *Nat. Catal.* **2019,** *2*, 648.
[3] Chia, X.; Pumera, M. *Nat. Catal.* **2018,** *1*, 909.
[4] Wang, L.; Zeng, Z.; Gao, W.; Maxson, T.; Raciti, D.; Giroux, M.; Pan, X.; Wang, C.; Greeley, J. *Science* **2019,** *363*, 870.

[5] Luo, M.; Zhao, Z.; Zhang, Y.; Sun, Y.; Xing, Y.; Lv, F.; Yang, Y.; Zhang, X.; Hwang, S.; Qin, Y.et al. *Nature* **2019,** *574*, 81.
[6] Qiu, Y.; Xin, L.; Li, Y.; McCrum, I. T.; Guo, F.; Ma, T.; Ren, Y.; Liu, Q.; Zhou, L.; Gu, S.et al. *J. Am. Chem. Soc.* **2018,** *140*, 16580.
[7] Qiao, B.; Wang, A.; Yang, X.; Allard, L. F.; Jiang, Z.; Cui, Y.; Liu, J.; Li, J.; Zhang, T. *Nat. Chem.* **2011,** *3*, 634.
[8] Yin, J.; Jin, J.; Lu, M.; Huang, B.; Zhang, H.; Peng, Y.; Xi, P.; Yan, C. H. *J. Am. Chem. Soc.* **2020,** *142*, 18378.
[9] Sun, M.; Dougherty, A. W.; Huang, B.; Li, Y.; Yan, C. H. *Adv. Energy Mater.* **2020,** *10*.
[10] Sun, M.; Wu, T.; Xue, Y.; Dougherty, A. W.; Huang, B.; Li, Y.; Yan, C.-H. *Nano Energy* **2019,** *62*, 754.
[11] Yang, X. F.; Wang, A.; Qiao, B.; Li, J.; Liu, J.; Zhang, T. *Acc. Chem. Res.* **2013,** *46*, 1740.
[12] Qin, R.; Liu, K.; Wu, Q.; Zheng, N. *Chem. Rev.* **2020,** *120*, 11810.
[13] Gao, X.; Liu, H.; Wang, D.; Zhang, J. *Chem. Soc. Rev.* **2019,** *48*, 908.
[14] Huang, C.; Li, Y.; Wang, N.; Xue, Y.; Zuo, Z.; Liu, H.; Li, Y. *Chem. Rev.* **2018,** *118*, 7744.
[15] Zhao, Y.; Wan, J.; Yao, H.; Zhang, L.; Lin, K.; Wang, L.; Yang, N.; Liu, D.; Song, L.; Zhu, J.et al. *Nat. Chem.* **2018,** *10*, 924.
[16] Yu, H.; Xue, Y.; Huang, B.; Hui, L.; Zhang, C.; Fang, Y.; Liu, Y.; Zhao, Y.; Li, Y.; Liu, H.et al. *iScience* **2019,** *11*, 31.
[17] Xue, Y.; Huang, B.; Yi, Y.; Guo, Y.; Zuo, Z.; Li, Y.; Jia, Z.; Liu, H.; Li, Y. *Nat. Commun.* **2018,** *9*, 1460.
[18] Hui, L.; Xue, Y.; Yu, H.; Liu, Y.; Fang, Y.; Xing, C.; Huang, B.; Li, Y. *J. Am. Chem. Soc.* **2019,** *141*, 10677.
[19] Yu, H.; Hui, L.; Xue, Y.; Liu, Y.; Fang, Y.; Xing, C.; Zhang, C.; Zhang, D.; Chen, X.; Du, Y.et al. *Nano Energy* **2020,** *72*.
[20] Yu, H.; Xue, Y.; Hui, L.; Zhang, C.; Fang, Y.; Liu, Y.; Chen, X.; Zhang, D.; Huang, B.; Li, Y. *Natl. Sci. Rev.***2020**, DOI:10.1093/nsr/nwaa213.
[21] Kaiser, S. K.; Chen, Z.; Faust Akl, D.; Mitchell, S.; Perez-Ramirez, J. *Chem. Rev.* **2020,** *120*, 11703.
[22] Hattori, H. *Chem. Rev.* **2002,** *95*, 537.
[23] Jeong, H.; Shin, S.; Lee, H. *ACS Nano* **2020,** *14*, 14355.
[24] Wang, H.; Liu, J. X.; Allard, L. F.; Lee, S.; Liu, J.; Li, H.; Wang, J.; Wang, J.; Oh, S. H.; Li, W.et al. *Nat. Commun.* **2019,** *10*, 3808.
[25] Zhang, X.; Chen, A.; Zhang, Z.; Zhou, Z. *J. Mater. Chem. A* **2018,** *6*, 18599.
[26] Tian, S.; Fu, Q.; Chen, W.; Feng, Q.; Chen, Z.; Zhang, J.; Cheong, W. C.; Yu, R.; Gu, L.; Dong, J.et al. *Nat. Commun.* **2018,** *9*, 2353.
[27] Zhao, J.; Zhao, J.; Li, F.; Chen, Z. *J. Phys. Chem. C* **2018,** *122*, 19712.
[28] Yang, Y.; Qian, Y.; Li, H.; Zhang, Z.; Mu, Y.; Do, D.; Zhou, B.; Dong, J.; Yan, W.; Qin, Y.et al. *Sci. Adv.* **2020,** *6*, eaba6586.
[29] Han, X.; Ling, X.; Yu, D.; Xie, D.; Li, L.; Peng, S.; Zhong, C.; Zhao, N.; Deng, Y.; Hu, W. *Adv. Mater.* **2019,** *31*, e1905622.
[30] Sun, M.; Wu, T.; Dougherty, A. W.; Lam, M.; Huang, B.; Li, Y.; Yan, C. H. *Adv. Energy Mater.* **2021,** *11*.
[31] Lu, Z.; Yadav, S.; Singh, C. V. *Catal. Sci. Technol.* **2020,** *10*, 86.
[32] Yu, X.; Han, P.; Wei, Z.; Huang, L.; Gu, Z.; Peng, S.; Ma, J.; Zheng, G. *Joule* **2018,** *2*, 1610.
[33] Tian, Y. H.; Hu, S.; Sheng, X.; Duan, Y.; Jakowski, J.; Sumpter, B. G.; Huang, J. *J. Phys. Chem. Lett.* **2018,** *9*, 570.

[34] Zhang, E.; Wang, T.; Yu, K.; Liu, J.; Chen, W.; Li, A.; Rong, H.; Lin, R.; Ji, S.; Zheng, X.et al. *J. Am. Chem. Soc.* **2019,** *141*, 16569.
[35] Qu, W.; Niu, S.; Sun, D.; Gao, H.; Wu, Y.; Yuan, Z.; Chen, X.; Wang, Y.; An, T.; Wang, G.et al. *Adv. Sci.* **2021,** *8*, 2002889.
[36] García, J.; Jiménez, C.; Martínez, F.; Camarillo, R.; Rincón, J. *J. Catal.* **2018,** *367*, 72.
[37] Han, N.; Wang, Y.; Yang, H.; Deng, J.; Wu, J.; Li, Y.; Li, Y. *Nat. Commun.* **2018,** *9*, 1320.
[38] Zu, X.; Li, X.; Liu, W.; Sun, Y.; Xu, J.; Yao, T.; Yan, W.; Gao, S.; Wang, C.; Wei, S.et al. *Adv. Mater.* **2019,** *31*, e1808135.
[39] Verboekend, D.; Keller, T. C.; Mitchell, S.; Pérez-Ramírez, J. *Adv. Funct. Mater.* **2013,** *23*, 1923.
[40] Liu, S.; Li, Z.; Wang, C.; Tao, W.; Huang, M.; Zuo, M.; Yang, Y.; Yang, K.; Zhang, L.; Chen, S.et al. *Nat. Commun.* **2020,** *11*, 938.
[41] Sun, M.; Dougherty, A. W.; Huang, B.; Li, Y.; Yan, C. H. *Adv. Energy Mater.* **2020**, *15*, 1903949.
[42] Hong, W. T.; Stoerzinger, K. A.; Lee, Y.-L.; Giordano, L.; Grimaud, A.; Johnson, A. M.; Hwang, J.; Crumlin, E. J.; Yang, W.; Shao-Horn, Y. *Energ. Environ. Sci.* **2017,** *10*, 2190.
[43] Grimaud, A.; May, K. J.; Carlton, C. E.; Lee, Y. L.; Risch, M.; Hong, W. T.; Zhou, J.; Shao-Horn, Y. *Nat. Commun.* **2013,** *4*, 2439.
[44] Quinonero-Candela, J. Q.; Rasmussen, C. E. *J. Mach. Learn. Res.* **2005,** *6*, 1939.
[45] Kaiser, S. K.; Chen, Z.; Faust Akl, D.; Mitchell, S.; Perez-Ramirez, J. *Chem. Rev.* **2020**, *120,* 11703.
[46] Fu, Q.; Saltsburg, H.; Flytzani-Stephanopoulos, M. *Science* **2003,** *301*, 935.
[47] Manna, K.; Ji, P.; Greene, F. X.; Lin, W. *J. Am. Chem. Soc.* **2016,** *138*, 7488.
[48] Mavrodinova, V.; Popova, M.; Mihályi, R. M.; Pál-Borbély, G.; Minchev, C. *Applied catalysis. A, General* **2003,** *248*, 197.
[49] Olson, D. H.; Khosrovani, N.; Peters, A. W.; Toby, B. H. *J. Phys. Chem. B* **2000,** *104*, 4844.
[50] van Bokhoven, J. A.; Lamberti, C. *Coord. Chem. Rev.* **2014,** *277-278*, 275.
[51] Yang, Y.; Zhang, L.; Hu, Z.; Zheng, Y.; Tang, C.; Chen, P.; Wang, R.; Qiu, K.; Mao, J.; Ling, T.et al. *Angew. Chem. Int. Ed. Engl.* **2020,** *59*, 4525.
[52] Chen, C.; Yan, D.; Wang, Y.; Zhou, Y.; Zou, Y.; Li, Y.; Wang, S. *Small* **2019,** *15*.
[53] Niu, S.; Jiang, W.-J.; Wei, Z.; Tang, T.; Ma, J.; Hu, J.-S.; Wan, L.-J. *J. Am. Chem. Soc.* **2019,** *141*, 7005.
[54] Zheng, Z.; Yu, L.; Gao, M.; Chen, X.; Zhou, W.; Ma, C.; Wu, L.; Zhu, J.; Meng, X.; Hu, J.et al. *Nat. Commun.* **2020,** *11*, 3315.
[55] Clark, S. J.; Segall, M. D.; Pickard, C. J.; Hasnip, P. J.; Probert, M. J.; Refson, K.; Payne, M. C. *Z. Kristallogr. Krist.* **2005,** *220*, 567.
[56] Perdew, J. P.; Burke, K.; Ernzerhof, M. *Phys. Rev. Lett.* **1996,** *77*, 3865.
[57] Hasnip, P. J.; Pickard, C. J. *Comput. Phys. Commun.* **2006,** *174*, 24.
[58] Perdew, J. P.; Chevary, J. A.; Vosko, S. H.; Jackson, K. A.; Pederson, M. R.; Singh, D. J.; Fiolhais, C. *Phys. Rev. B* **1992,** *46*, 6671.
[59] Vanderbilt, D. *Phys. Rev. B* **1990,** *41*, 7892.
[60] Head, J. D.; Zerner, M. C. *Chem. Phys. Lett.* **1985,** *122*, 264.
[61] Probert, M. I. J.; Payne, M. C. *Phys. Rev. B* **2003,** *67*.
[62] Rodriguez, J. D.; Perez, A.; Lozano, J. A. *IEEE Trans. Pattern Anal. Mach. Intell.* **2010,** *32*, 569.

The introduction of main group elements in the atomic catalysts still lack in-depth understanding. In this work, we have introduced the main group elements as efficient modulators via the s-p-d orbital couplings in GDY-based DAC regarding both thermodynamic stability and electroactivity. This work further opens up new development directions for future DAC in broad applications.

M. Sun, H. H. Wong, T. Wu, A. W. Dougherty, B. Huang*

Stepping out of Transition Metals: Activating the Dual Atomic Catalyst through Main Group Elements

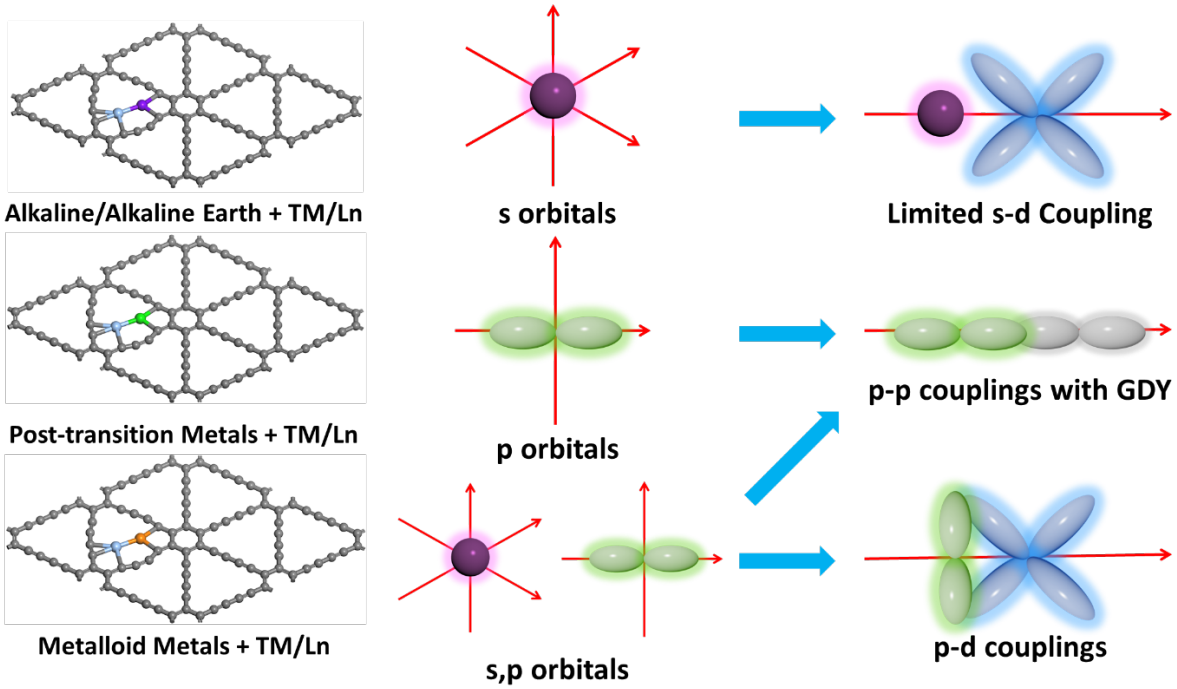

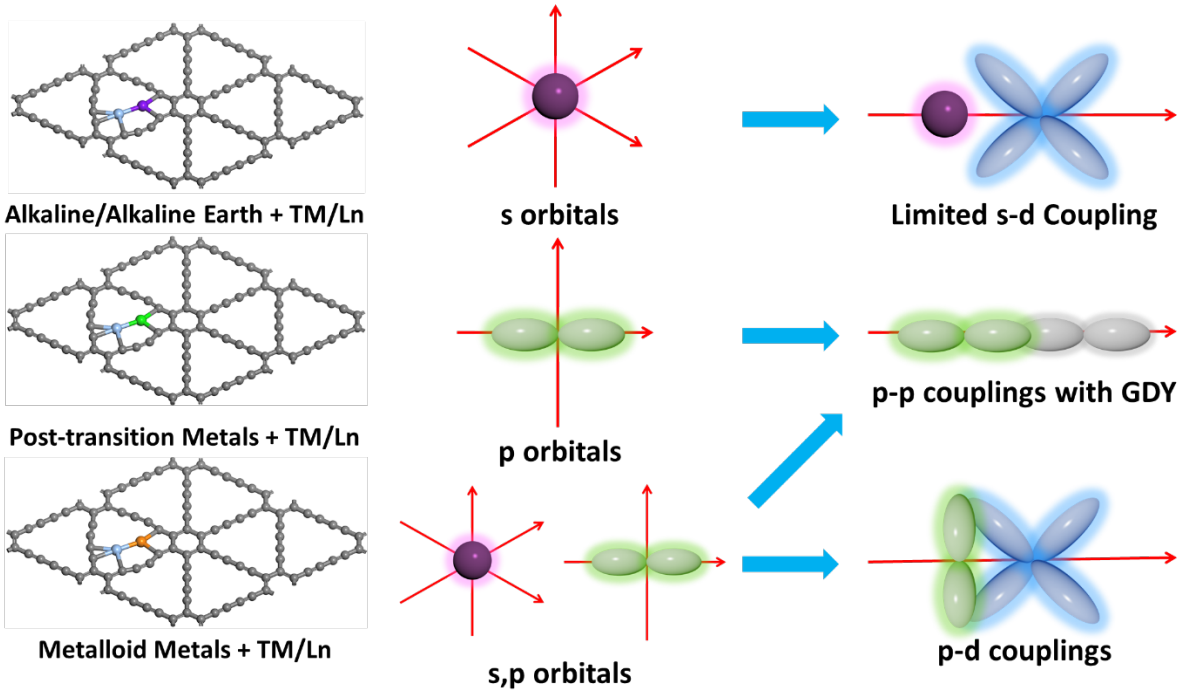

Figure 1. The schematic diagram of the main group elements based GDY-DAC. The varied dominant orbitals lead to different interactions with transition metals or lanthanide metals, which further results in distinct thermodynamic stability and electronic structure modulations.

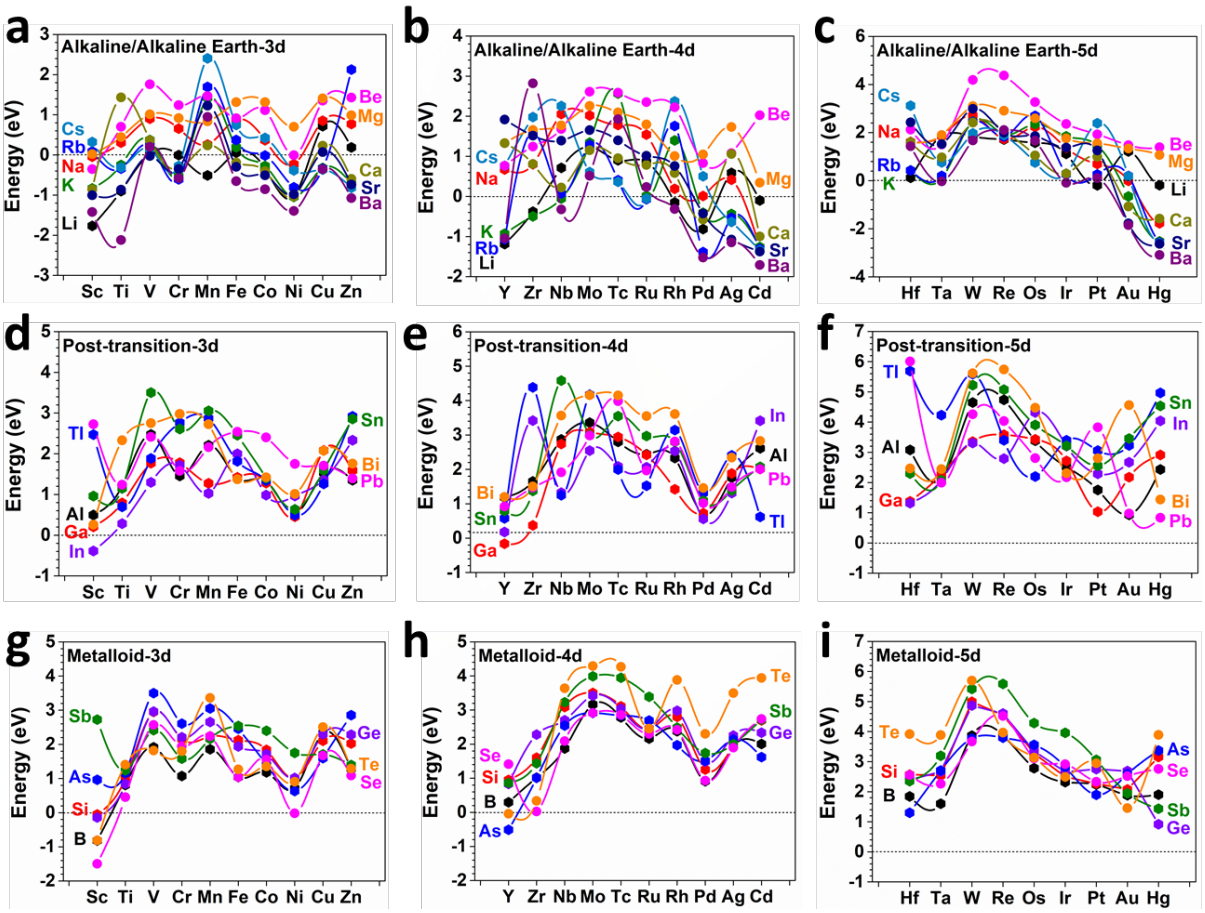

Figure 2. The formation energy of main group elements-based GDY-DAC. The formation energies of GDY-based DAC by combinations of alkaline/alkaline earth metals and transition metals (a) 3d, (b) 4d, and (c) 5d. The formation energies of GDY-based DAC by combinations of post-transition metals and transition metals (d) 3d, (e) 4d, and (f) 5d. The formation energies of GDY-based DAC by combinations of metalloid and transition metals (g) 3d, (h) 4d, and (i) 5d.

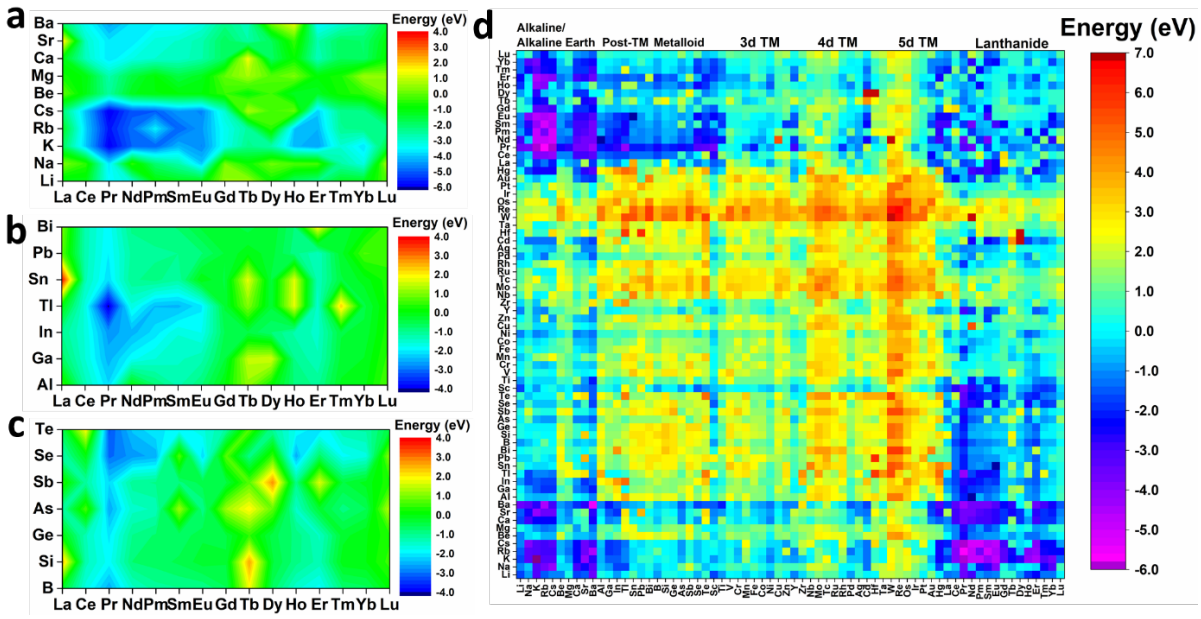

Figure 3. The energy mapping of GDY-DAC. (a) The formation energies of GDY-based DAC by combinations of AAEM and Ln metals. (b) The formation energies of GDY-based DAC by combinations of Post-TM and Ln metals. (c) The formation energies of GDY-based DAC by combinations of metalloid and Ln metals. (d) The formation energy mapping of all the combinations for transition metals, lanthanide metals, AAEM, Post-TM, and metalloid elements.

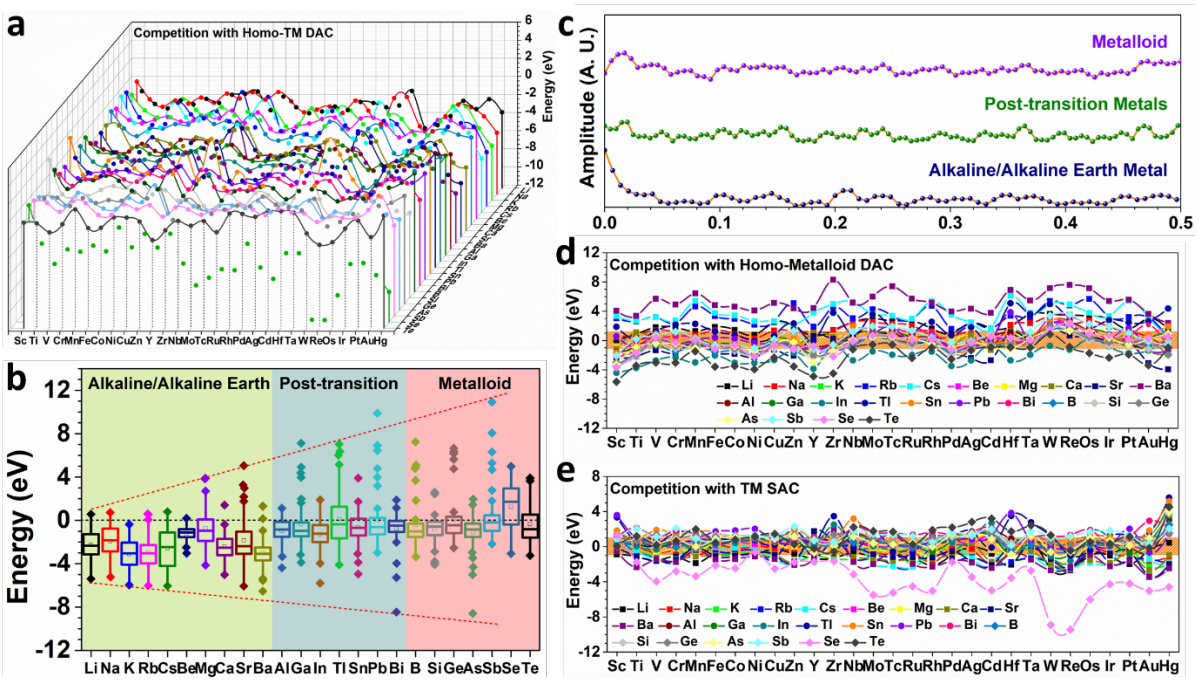

Figure 4. The energy competitions in GDY-DAC. (a) The formation energy comparison between hetero-alkaline/alkaline earth, post-transition metals, and metalloids based GDY-DAC and homo-TM DAC. (b) The boxing plot of formation energy for GDY-DAC with combinations between alkaline/alkaline earth, post-transition metals, metalloids, and transition metals. (c) The FFT transfer of formation energies in (b). (d) The formation energy comparison between hetero- and homo- alkaline/alkaline earth, post-transition metals, and metalloids based GDY-DAC. (e) The formation energy comparison between hetero-alkaline/alkaline earth, post-transition metals, and metalloids based GDY-DAC and TM-based GDY-SAC.

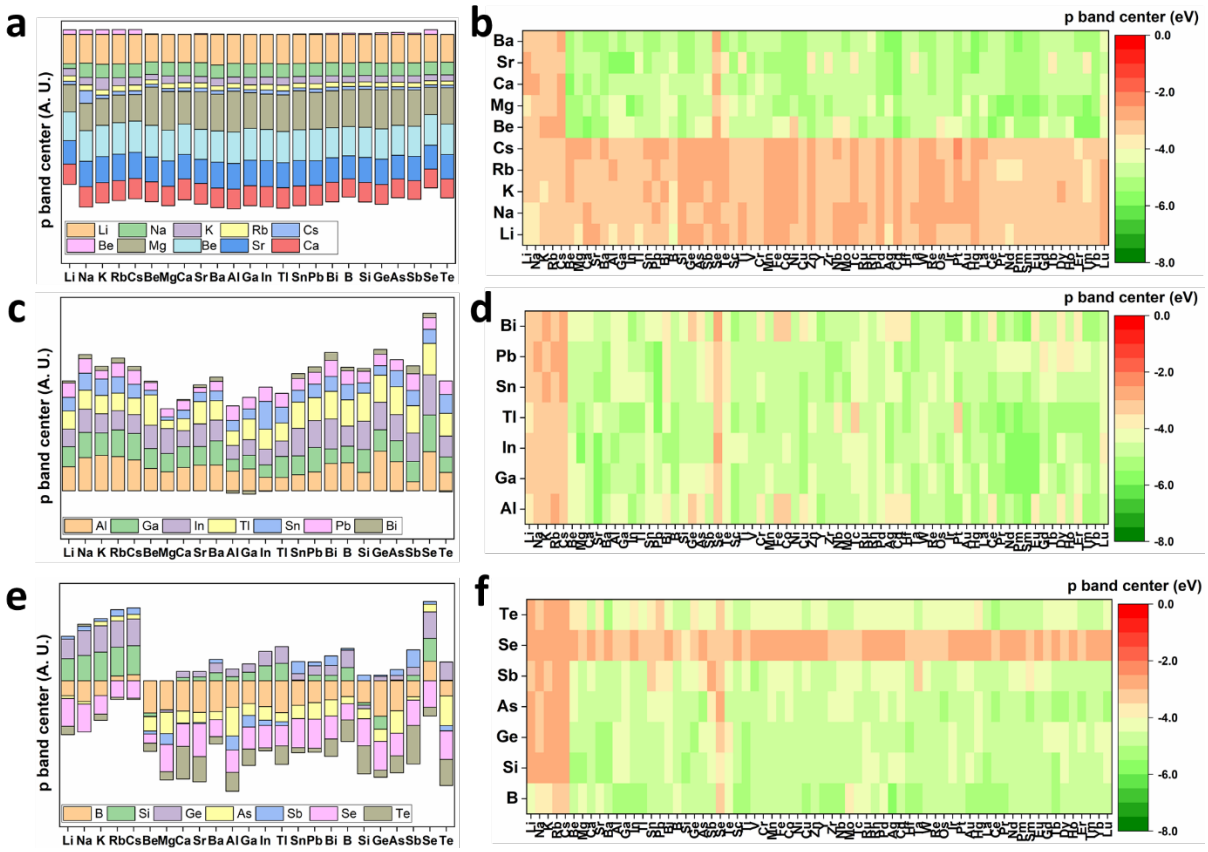

Figure 5. The p-band center variations in GDY-DAC. (a) The p-band center of alkaline/alkaline earth metals in the GDY-DAC. (b) The p-band center of alkyl chain in the alkaline/alkaline earth, post-transition metals, and metalloids based GDY-DAC. (c) The p-band center of post-transition metals in the GDY-DAC. (d) The p-band center of the alkyl chain in the post-transition metals based GDY-DAC. (e) The p-band center of metalloid in the GDY-DAC. (f) The p-band center of the alkyl chain in the metalloid based GDY-DAC.

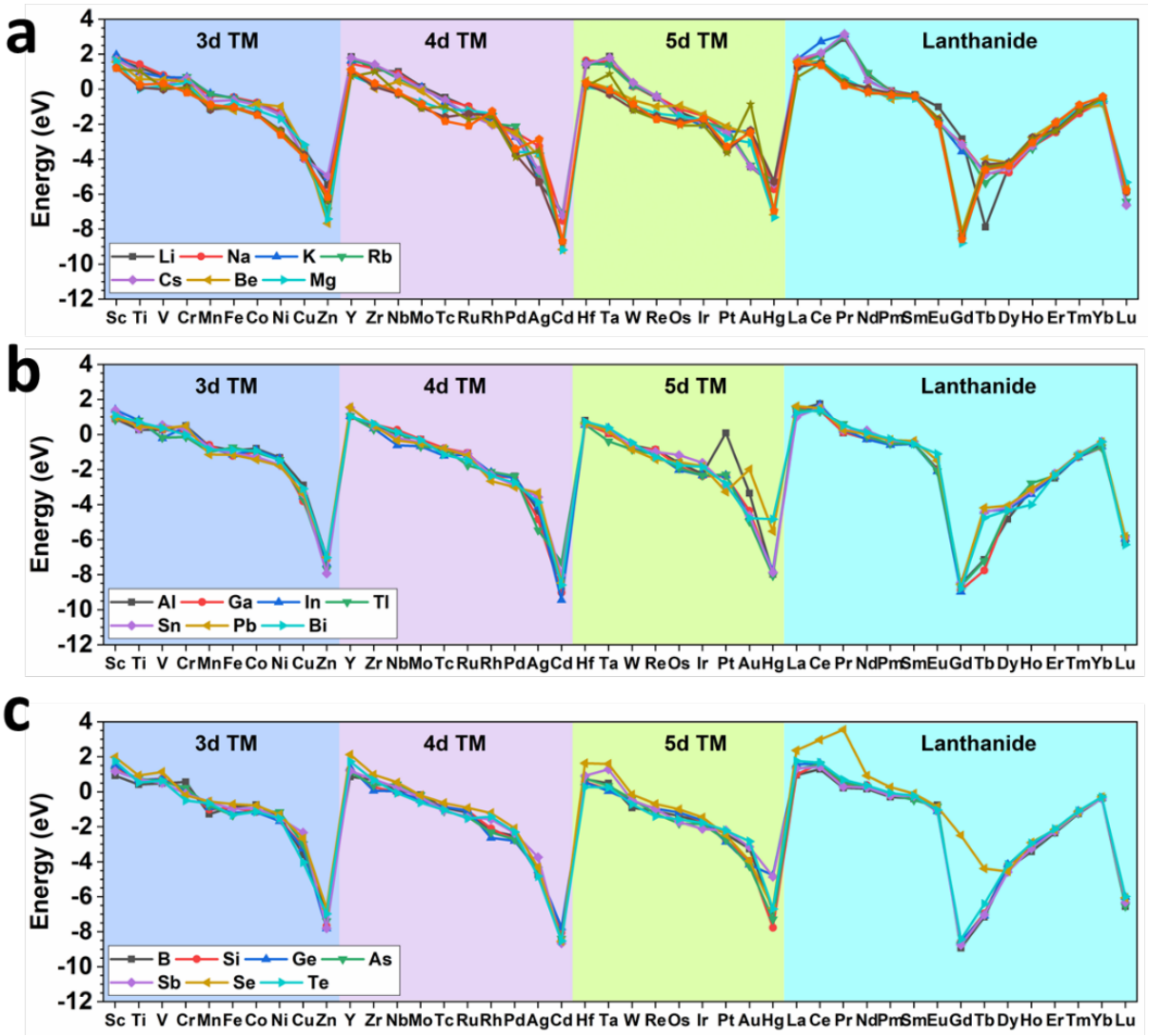

Figure 6. The d/f-band center variations in GDY-DAC. (a) The d/f-band center of transition metals/lanthanide metals in the alkaline/alkaline earth metal based GDY-DAC. (b) The d/f-band center of transition metals/lanthanide metals in the post-transition metal based GDY-DAC. (c) The d/f-band center of transition metals/lanthanide metals in the metalloid earth metal based GDY-DAC.

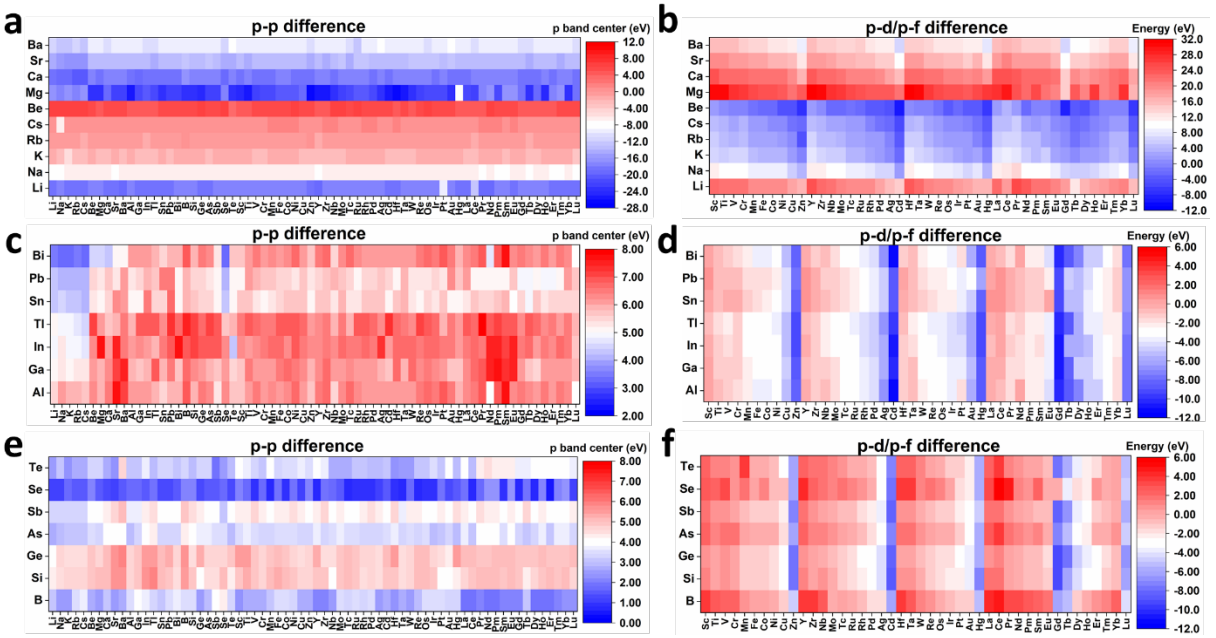

Figure 7. The orbital coupling effect in GDY-DAC. (a) The p-band center difference between alkaline/alkaline earth metals and all the elements and in the GDY-DAC. (b) The difference between the p-band center of alkaline/alkaline earth metals and the d/f-band center of transition metals and lanthanide metals in the GDY-DAC. (c) The p-band center difference between post-transition metals and all the elements and in the GDY-DAC. (d) The difference between the p-band center of post-transition metals and d/f-band center of transition metals and lanthanide metals in the GDY-DAC. (e) The p-band center difference between metalloids and all the elements and in the GDY-DAC. (f) The difference between the p-band center of metalloids and d/f-band center of transition metals and lanthanide metals in the GDY-DAC.

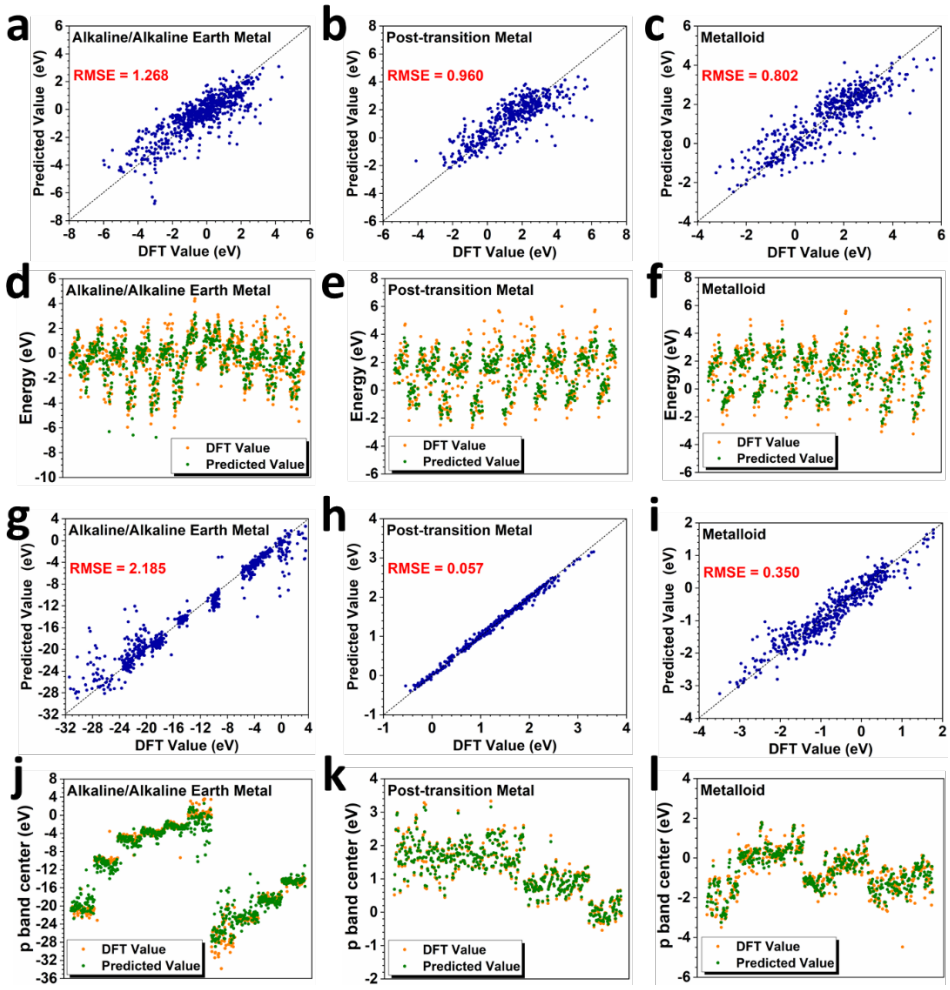

Figure 8. GPR-based machine learning predictions on formation energies and p=band centers of GDY-DAC. (a,d) The comparison and scattering plot of the GPR model predicted data and original data of the formation energy in alkaline/alkaline earth metals based GDY-DAC. (b,e) The comparison and scattering plot of the GPR model predicted data and original data of the formation energy in post-transition metals based GDY-DAC. (c,f) The comparison and scattering plot of the GPR model predicted data and original data of the formation energy in metalloid based GDY-DAC. (g,j) The comparison and scattering plot of the GPR model predicted data and original data of the p-band center in post-transition metals based GDY-DAC. (h,k) The comparison and scattering plot of the GPR model predicted data and original data of the p-band center in post-transition metals based GDY-DAC. (i,l) The comparison and scattering plot of the GPR model predicted data and original data of the p-band center in metalloid based GDY-DAC.